Nanomechanical Measurement of Magnetostriction and Magnetic Anisotropy in (Ga,Mn)As

S. C. Masmanidis,[1] H. X. Tang,[1] E. B. Myers,[1] Mo Li,[1] K. De Greve,[1,2] G. Vermeulen,[1,2] W. Van Roy,[2] and M. L. Roukes[1]

[1]*Condensed Matter Physics 114-36, California Institute of Technology, Pasadena, California 91125, USA*

[2]*IMEC, Kapeldreef 75, B-3001 Leuven, Belgium*

(Received 5 May 2005; published 28 October 2005)

A GaMnAs nanoelectromechanical resonator is used to obtain the first measurement of magnetostriction in a dilute magnetic semiconductor. Resonance frequency shifts induced by field-dependent magnetoelastic stress are used to simultaneously map the magnetostriction and magnetic anisotropy constants over a wide range of temperatures. Owing to the central role of carriers in controlling ferromagnetic interactions in this material, the results appear to provide insight into a unique form of magnetoelastic behavior mediated by holes.

DOI: 10.1103/PhysRevLett.95.187206 PACS numbers: 75.80.+q, 75.50.Pp, 75.70.−i, 85.85.+j

The dilute magnetic semiconductor (DMS) GaMnAs has been extensively studied for its promising spintronics applications [1,2]. Among its properties is the dominant role of growth-induced strain upon the material's magnetic alignment. A change from compressive to tensile strain is known to flip the moments from in plane to out of plane [1]. This is consistent with the inverse magnetoelastic effect, but the magnetoelastic coupling parameters that quantify this behavior have remained elusive. These parameters are important in gauging the impact of magnetostriction on magnetic [3] and electrical transport properties [4,5], and are therefore essential to a comprehensive understanding of DMS systems. Here, we demonstrate a scheme to observe magnetostriction directly in a resonant nanoelectromechanical system (NEMS). Similarities between the piezoresistive, piezoelectric, and elastic properties of GaMnAs to conventionally doped GaAs enable straightforward electromechanical actuation and transduction [6,7] of a doubly clamped beam resonator. Mechanical resonance frequency variations occur as the device is stretched or compressed magnetoelastically in an applied magnetic field, providing a measure of magnetostriction with an accuracy comparable to other methods [8,9]. Furthermore, the angular dependence of the observed magnetostriction enables measurement of another important property, magnetic anisotropy.

The material is grown epitaxially on an (001) GaAs substrate, beginning with a 1 μm $Al_{0.8}Ga_{0.2}As$ sacrificial layer, followed by 50 nm high temperature and 50 nm low temperature GaAs, and finally 80 nm unannealed $Ga_{0.948}Mn_{0.052}As$ with a Curie temperature of $\sim$57 K. The spontaneous magnetization is expected to lie in the growth plane due to a compressive strain from the substrate and demagnetization effects. Electron beam lithography is used to define the device profile, which is subsequently covered with a titanium etch mask. Next, argon ion milling removes all magnetic material not protected by the mask. A 30 nm-thick gold side gate is deposited 0.7 μm away from the beam after another lithography step. Finally, a rectangular resist window is patterned to expose the sacrificial layer, which is selectively removed along with the remaining titanium mask in dilute hydrofluoric acid. The resulting suspended structure, shown in the inset of Fig. 1(a), has dimensions of $(L, w, t) = (6, 0.5, 0.18)$ μm, with its longitudinal axis oriented along the [110] crystallographic direction. The sample is mounted in a liquid helium cryostat in vacuum, and surrounded by a 3-axis, 10 kOe superconducting magnet.

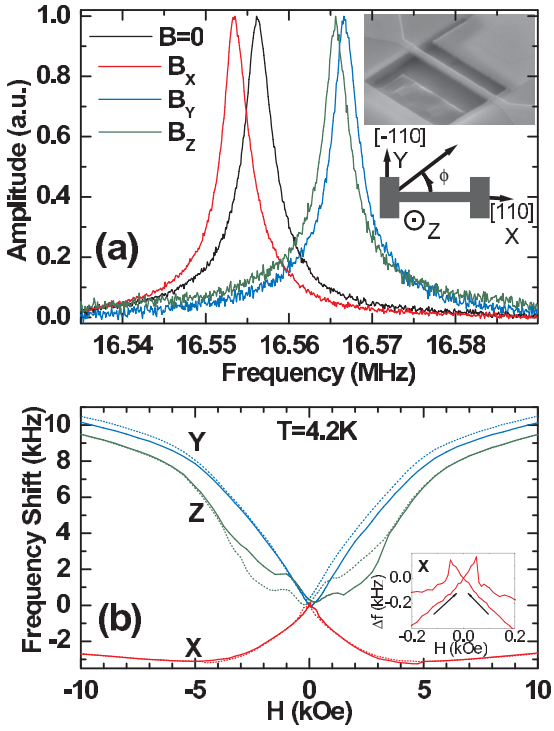

FIG. 1 (color). (a) Frequency response of the device for various 10 kOe field directions (Z is out of the plane). Amplitude is normalized for clarity. Inset: SEM image of the suspended GaMnAs beam and Au side gate with the axis directions. (b) Frequency shift dependence on field magnitude and direction. Dotted curves are for reversed field sweep direction. Inset: Expanded view of shifts in a field along X, showing domain wall-induced transitions.

The two-terminal device resistance at 4.2 K is 80 kΩ. By applying an ac voltage on the side gate, a piezoelectric dipole interaction [6] drives the beam out of plane in its fundamental resonance mode. Transduction is carried out via a sensitive piezoresistive down-mixing scheme [7] with the signal detected using a lock-in amplifier, following low noise preamplification.

The piezoresistive frequency response along different magnetic field directions is shown in Fig. 1(a). At 4.2 K and zero external field, the device resonates at 16.56 MHz with a quality factor of 6300. The resonance is tuned up or down, depending on whether the applied field is aligned parallel or orthogonal to the [110] direction. We attribute these shifts to magnetoelastic stress that stretches or compresses the beam. Note that torque-induced shifts [10] that are prevalent in larger devices are not expected to have a significant impact on the resonance of the smaller, stiffer DMS device studied here.

The device can be operated as part of a phase-locked loop (PLL), enabling real-time resonance frequency tracking with a resolution of 4 parts in 10^7 at 4.2 K. Figure 1(b) shows the frequency shifts as a function of field along the three principal beam directions. Experimentally one can identify three distinct tuning regions corresponding to low ($<$100 Oe), intermediate (100–5000 Oe) and high ($>$5000 Oe) field behavior. In the low field region magnetization reversal appears to proceed via domain wall displacement, characterized by abrupt changes in frequency as shown in the Fig. 1(b) inset. The intermediate region apparently coincides with coherent moment rotation described by the Stoner-Wohlfarth model [11]. Note that hysteresis can be found in the first two regions. The magnetization reversal is complete beyond ~5000 Oe, but frequency continues to increase with field. This last observation is consistent with a forced magnetostriction effect [12]. The field dependence measurements are extended to higher temperatures in Fig. 2. For clarity, only the results for a field oriented in plane and orthogonal to the beam are displayed. The magnitude of the frequency shift decreases with temperature, and a small parastrictive effect persists above the Curie point up to at least 65 K. Starting at 20 K a downshift in frequency occurs at low and intermediate fields, suggesting qualitative changes occur in magnetostriction as a function of temperature. The slope of the high field, linear part of the curves provides a rough gauge of the forced magnetostriction. We find that this effect decreases with temperature and vanishes at around 60 K. The concurrent onset of forced magnetostriction and ferromagnetic ordering in our sample confirms that this phenomenon is intrinsic to GaMnAs, and may be associated with a field-dependent magnetization that remains unsaturated above 1 T [13,14]. A more systematic study of these effects requires higher magnetic fields, and falls beyond the scope of this work.

To gain a better understanding of magnetoelastic coupling we use a PLL to track resonance frequency shifts in a constant field that is rotated in the plane of the device. The

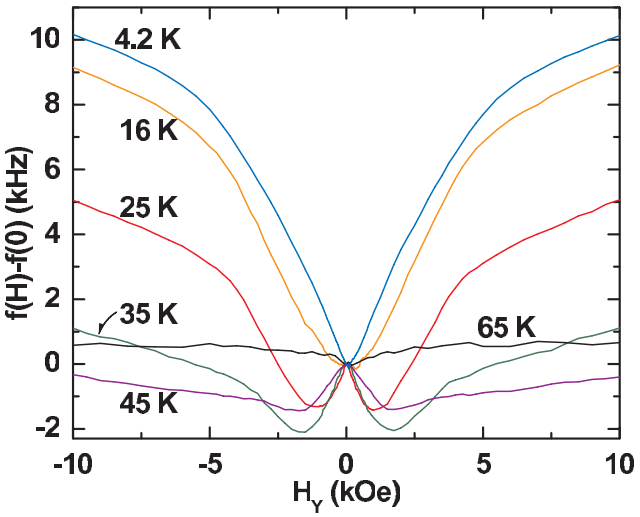

FIG. 2 (color). Frequency shift dependence on a field along $\phi_H = 90°$ for different temperatures.

results are presented in polar form in Fig. 3, with the field chosen as 5 kOe such that magnetization reversal occurs purely by rotation, i.e., no domain wall displacement. Forced magnetostriction effects will also be curtailed at this intermediate field value. The field angle ϕ_H is measured with respect to the [110] direction. Between 4.2 and 20 K we see a twofold symmetry in the angular dependence of the resonance frequency, which is maximized

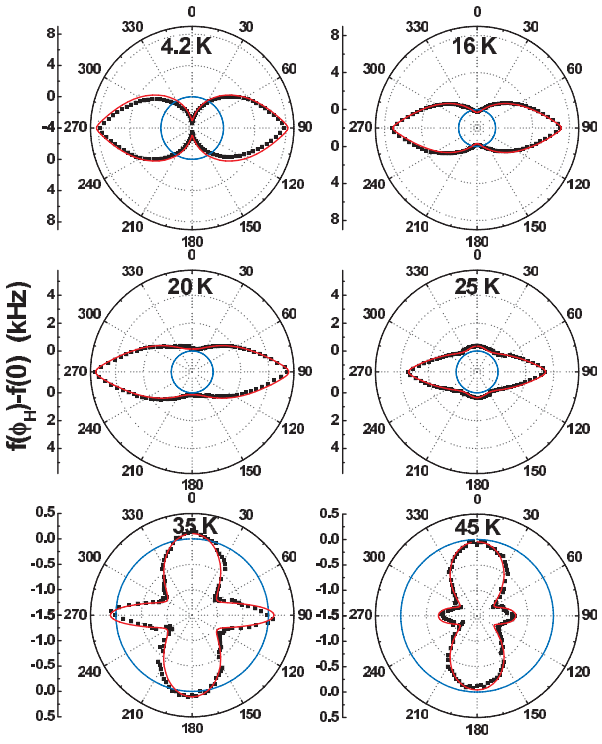

FIG. 3 (color). Polar plot of angular dependence of frequency shifts for an in-plane 5 kOe field. The field angle is measured relative to [110]. The $\Delta f = 0$ reference lines are shown in blue. The red curves are fits to the magnetoelastic stress model.

along 90° and 270°, and minimized along 0° and 180°. However, by 25 K, additional symmetry emerges in the form of two new peaks at 0° and 180°. The new peaks grow with temperature relative to the original pair, and above 35 K they are the dominant feature of angular dependence in Fig. 3. This behavior suggests qualitative changes in magnetoelastic coupling and anisotropy occur with increasing temperature.

We now attempt to extract quantitative information from the data in Fig. 3. The angular dependence of the frequency shifts is modeled after the magnetostriction equation [12,15] containing the first order terms λ_{100} and λ_{111} corresponding to volume-conserving deformations, and a second order term h_3 corresponding to a volume-changing deformation. The twofold or fourfold symmetry found in the polar plots can be uniquely and unambiguously described by first and second order magnetostriction. Combining this model with the stress-strain relation gives the following expression for the excess longitudinal magnetoelastic stress on the beam relative to the zero field stress:

$$\sigma_{ML} = (\lambda_{100}/4)(c_{11} - c_{12}) + (3\lambda_{111}/4)(c_{11} - c_{12}) \times \cos 2\phi_M + (h_3/4)(c_{11} + 2c_{12})\cos^2 2\phi_M \quad (1)$$

where ϕ_M is the in-plane magnetization angle. The inclusion of the second order term is necessary to explain the fourfold symmetry seen above 20 K. The precise elastic constants of $Ga_{0.948}Mn_{0.052}As$ are unknown but assumed to be very similar to those of GaAs: $c_{11} = 121.6$ GPa, $c_{12} = 54.5$ GPa and Young's modulus $E = 86$ GPa [16]. We rely on a finite element simulation to model the beam's dynamics upon stressing the 80 nm-thick magnetic top layer of the beam. For the range of relevant magnetoelastic strain, the model predicts a linear stress-frequency gauge factor that for the specific device geometry used here is equal to $\Delta f/\Delta\sigma_{ML} = -13.9$ Hz/kPa.

We find it necessary to include a cubic and in-plane uniaxial magnetic anisotropy in our model in order to quantitatively describe the curvature of the angular dependence of frequency in Fig. 3. The Stoner-Wohlfarth model is used to couple the magnetoelastic stress equation, expressed in terms of the magnetization angle, to the frequency shifts which are measured with respect to the field angle. The corresponding minimum free energy condition is [17]

$$H_{KU}\sin 2\phi_M - (H_{K1}/2)\sin 4\phi_M + 2H\sin(\phi_M - \phi_H) = 0. \quad (2)$$

The first order in-plane uniaxial and cubic anisotropy fields are given by $H_{KU} = 2K_U/M$ and $H_{K1} = 2K_1/M$. We ignore the magnetoelastic second order anisotropy contribution to free energy, because this varies as $\sim E\lambda^2\cos^4\phi_M$ and can be disregarded for small λ. With this assumption, Eqs. (1) and (2) are effectively coupled via a single variable ϕ_M, enabling extraction of the magnetostriction and anisotropy parameters by a straightforward best fit analysis. First, the three magnetostriction constants are obtained by applying the stress-frequency gauge factor on Eq. (1) and fitting to the frequency shift maxima and minima that occur in Fig. 3 at multiples of $\phi_M = 90°$. The magnetization is independent of anisotropy along these field directions. To obtain H_{KU} and H_{K1}, Eq. (2) is fed into Eq. (1) after being solved with trial anisotropy constants, and the procedure is iterated to produce the best fit to the data. The fits are included in Fig. 3. We find this method quantitatively explains the angular dependence of the frequency shifts over the entire ferromagnetic regime, up to the Curie transition near 57 K. The experimentally derived magnetostriction and magnetic anisotropy field parameters are plotted in Figs. 4(a) and 4(b). At 4.2 K, the first order magnetostriction constants of $Ga_{0.948}Mn_{0.052}As$ along [100] and [111] are $\lambda_{100} = -11.3$ parts per million (ppm) and $\lambda_{111} = 8.1$ ppm, respectively. The measured anisotropy fields are the same order of magnitude as those from studies on bulk GaMnAs films [18,19]. Based upon the range of parameters that fit the model, our results are accurate to within ± 0.1 ppm and ± 0.3 kOe in magnetostriction and anisotropy, respectively. The larger relative error in anisotropy reflects the more indirect coupling between that quantity and mechanical resonance frequency.

The temperature dependence displayed in Fig. 4 reveals an intricate coupling between magnetostriction and mag-

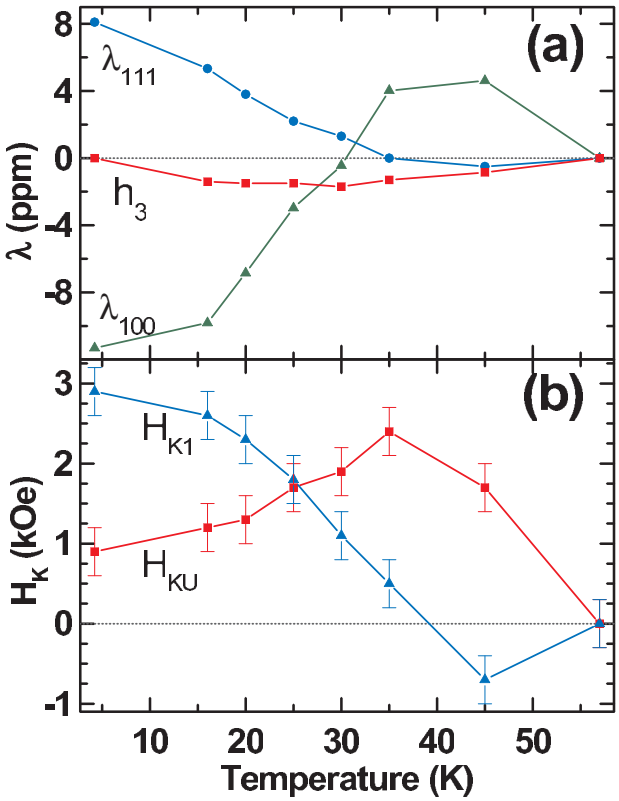

FIG. 4 (color). (a) First and second order magnetostriction constants of $Ga_{0.948}Mn_{0.052}As$. (b) First order cubic and in-plane uniaxial anisotropy fields.

netic anisotropy. At 4.2 K both H_{KU} and H_{K1} are positive and $H_{K1} > H_{KU}$, indicating the magnetization lies in the (001) plane with cubic easy axis symmetry close to [100] and [010]. The uniaxial anisotropy tips the moments in the direction of [110] by $0.5\sin^{-1}(H_{KU}/H_{K1}) = 9°$ [17]. The magnitude of the tilting angle gradually increases and by 25 K, complete realignment along [110] has occurred accompanied by a changeover to uniaxial easy axis symmetry. It is notable that the same transition is observed elsewhere [18]. The span between 30 and 40 K is marked by significant qualitative changes in all measured parameters. Specifically, λ_{100} and λ_{111} change sign while H_{KU} and h_3 attain their respective local maximum and minimum values. The trend of H_{K1} suggests it changes sign at around 40 K. Above this temperature, the device still retains its uniaxial easy axis symmetry along [110], since $|H_{KU}| > |H_{K1}|$.

The sign change of cubic anisotropy with increasing temperature appears to be consistent with models of carrier-mediated ferromagnetism in DMS [20,21]. These, and apparently related observations [22,23], may be the result of a thermally driven increase in hole density. Magnetostriction, like anisotropy, arises from interactions between neighboring magnetic moments and, consequently, it is also expected to be coupled to the carrier density. This is supported by the similar temperature dependence observed between magnetostriction and anisotropy in Fig. 4. Moreover, the dependence of valence band energy on strain leads us to expect a sensitive interplay between hole density, magnetic anisotropy, magnetostriction, and other sources of strain in dilute magnetic semiconductors. Lattice thermal expansion, in particular, may play a role in this process, as it changes sign [24] in the temperature regime relevant to DMS, and is known to vary with carrier density [25].

The inverse magnetoelastic contribution to anisotropy can be approximated as a field of the form $H_{KU}^{\sigma} \sim -3\lambda_i \varepsilon_i E/M$ [12], where ε_i is the strain along a specified direction. A tetragonal distortion of $Ga_{0.948}Mn_{0.052}As$ grown on GaAs would lead us to expect an in-plane biaxial anisotropy along the [110] and equivalent axes. However, asymmetric strain from surface reconstruction [26], as well as from device bending, would tend to favor uniaxial anisotropy. Using the above estimate, with the experimental value for λ_{110} given by [12] $\lambda_{100}/4 + 3\lambda_{111}/4 = 3.2$ ppm, and $M_S \approx 0.05$ T, we find that a strain of $-0.4 \pm 0.1\%$ along [110] reproduces the measured value of H_{KU} at 4.2 K. This closely coincides with the -0.3% strain reported for $Ga_{0.948}Mn_{0.052}As$ grown on top of GaAs [1], suggesting that inverse magnetostriction is an important source of magnetic anisotropy in this system.

In summary, we have employed a NEMS resonator to measure the magnetostriction constants and magnetic anisotropy fields of GaMnAs. We observe a gradual temperature-driven crossover at 25 K from in-plane cubic to uniaxial easy axis symmetry. At even higher temperatures all parameters undergo qualitative changes that reveal a pronounced coupling between magnetoelastic effects and magnetic anisotropy. This appears to provide experimental evidence for hole-mediated magnetostriction in dilute magnetic semiconductors. Both hole concentration and spin polarization appear to influence magnetoelastic coupling in DMS. Strain may play a key role in the carrier modulation process, thereby indirectly impacting magnetostriction and magnetic anisotropy, and also directly giving rise to substantial inverse magnetoelastic anisotropy fields. This raises the prospect for engineering DMS devices that rely on externally applied stress to achieve novel control and tunability of magnetic and electronic behavior.

This work was supported by DARPA under grant No. DSO/SPINS-MDA 972-01-1-0024. K. D. G. acknowledges support as research assistant of the Research Fund Flanders (FWO).

[1] H. Ohno, Science **281**, 951 (1998).
[2] S. A. Wolf *et al.*, Science **294**, 1488 (2001).
[3] J. A. Schuler *et al.*, J. Appl. Phys. **95**, 4922 (2004).
[4] C. Ruester *et al.*, Phys. Rev. Lett. **91**, 216602 (2003).
[5] O. Ozatay *et al.*, J. Appl. Phys. **95**, 7315 (2004).
[6] H. X. Tang *et al.*, Appl. Phys. Lett. **81**, 3879 (2002).
[7] I. Bargatin *et al.*, Appl. Phys. Lett. **86**, 133109 (2005).
[8] E. Klokholm, IEEE Trans. Magn. **12**, 819 (1976).
[9] A. C. Tam and H. Schroeder, J. Appl. Phys. **64**, 5422 (1988).
[10] J. G. E. Harris *et al.*, Appl. Phys. Lett. **75**, 1140 (1999).
[11] E. C. Stoner and E. P. Wohlfarth, Phil. Trans. R. Soc. A **240**, 599 (1948).
[12] S. Chikazumi, *Physics of Magnetism* (Wiley, New York, 1964).
[13] A. Oiwa *et al.*, Solid State Commun. **103**, 209 (1997).
[14] V. F. Sapega *et al.*, Phys. Rev. Lett. **94**, 137401 (2005).
[15] R. Becker and W. Döring, *Ferromagnetismus* (Springer Verlag, Berlin, 1939), p. 136.
[16] R. I. Cottam and G. A. Saunders, J. Phys. C **6**, 2105 (1973).
[17] H. X. Tang *et al.*, Phys. Rev. Lett. **90**, 107201 (2003).
[18] U. Welp *et al.*, Phys. Rev. Lett. **90**, 167206 (2003).
[19] X. Liu, Y. Sasaki, and J. K. Furdyna, Phys. Rev. B **67**, 205204 (2003).
[20] M. Abolfath, T. Jungwirth, J. Brum, and A. H. MacDonald, Phys. Rev. B **63**, 054418 (2001).
[21] T. Dietl, H. Ohno, and F. Matsukura, Phys. Rev. B **63**, 195205 (2001).
[22] M. Sawicki *et al.*, J. Supercond. **16**, 7 (2003).
[23] M. Sawicki *et al.*, Phys. Rev. B **71**, 121302 (2005).
[24] P. W. Sparks and C. A. Swenson, Phys. Rev. **163**, 779 (1967).
[25] M. Cardona and N. E. Christensen, Phys. Rev. B **35**, 6182 (1987).
[26] Y. B. Xu, D. J. Freeland, M. Tselepi, and J. A. C. Bland, Phys. Rev. B **62**, 1167 (2000).